Submitted to Physical Review

UCRL-19305
Preprint

FOUR-BODY STRANGE PARTICLE PRODUCTION IN pp COLLISIONS AT 6 BeV/c

S. Klein, W. Chinowsky, R. R. Kinsey, M. Mandelkern,
J. Schultz and T. H. Tan

October 1969

AEC Contract No. W-7405-eng-48

LAWRENCE RADIATION LABORATORY
UNIVERSITY of CALIFORNIA BERKELEY

UCRL-19305

DISCLAIMER

FOUR-BODY STRANGE PARTICLE PRODUCTION IN pp COLLISIONS AT 6 BeV/c*

S. Klein,‡ W. Chinowsky, R. R. Kinsey,‡
M. Mandelkern,+ and J. Schultz+

Physics Department and Lawrence Radiation Laboratory,
University of California, Berkeley, California

and

T. H. Tan++

Stanford Linear Accelerator Center, Stanford, California

ABSTRACT

An exposure of the LRL 72-in. liquid-hydrogen bubble chamber to 6 BeV/c protons has yielded some 3000 examples of production of strange particles in four-body final states. Cross sections for the reactions $pp \to \Lambda pK^0\pi^+$, $pp \to \Lambda pK^+\pi^0$, and $pp \to \Lambda nK^+\pi^+$ are 64 ± 6 μb, 39 ± 6 μb, and 43 ± 4 μb, respectively. The resonances K*(890), N*(1236), and Y*(1385) are produced with cross sections

$$\sigma(pK^{*+}) = 9 \pm 3 \text{ μb}$$
$$\sigma(\Lambda K^0 N^{*++}) = 23 \pm 3 \text{ μb}$$
$$\sigma(\Lambda K^+ N^{*+}) = 4 \pm 2 \text{ μb}$$
$$\sigma(pK^0 Y^{*+}) = 11 \pm 2 \text{ μb}$$
$$\sigma(pK^+ Y^{*0}) = 7 \pm 1 \text{ μb}$$
$$\sigma(nK^+ Y^{*+}) = 15 \pm 2 \text{ μb}$$

Except for the low Kπ effective mass region, the data are found to be in good agreement with a pion exchange model.

---

* Work performed under the auspices of the U. S. Atomic Energy Commission.

‡ Present address: Universität Heidelberg, Heidelberg, Germany.

‡ Present address: Brookhaven National Laboratory, Upton, New York.

+ Present address: University of California, Irvine.

++ Present address: University of Colorado, Boulder, Colorado.

I. INTRODUCTION

The inelastic proton-proton interaction[1] has been studied most extensively in reactions yielding non-strange particles. Those results indicate that resonance production is dominant and that the reactions can often be interpreted as examples of pseudo-two-body production. Single pion exchange models have been generally successful in interpreting these data. Until recently, the strange particle data have been too sparse for any detailed analysis. The three-body strange particle final states have been investigated and the reported results indicate that pion exchange is probably an important mechanism in their production.[2-8] The four-body strange states have been only incompletely or qualitatively studied previously.[2,3,5]

We present results for the reactions

$$pp \rightarrow \Lambda p K^0 \pi^+ \qquad \text{(a)}$$

$$\Lambda p K^+ \pi^0 \qquad \text{(b)}$$

$$\Lambda n K^+ \pi^+ \qquad \text{(c)}$$

produced by 6 BeV/c protons incident on the Alvarez 72" liquid hydrogen bubble chamber. Details of the 550,000 picture exposure at the Bevatron at LRL have been presented in another paper[4] reporting results of the experiment and will not be repeated here. We find Y*(1385) resonance production in all three final states and N*(1236) and K*(890) production in reactions (a) and (b). A low mass enhancement in the Y*K system is observed in all reactions and has been interpreted as N*(1950) production proceeding via pion exchange. The latter result has been previously reported.[9]

II. PROCESSING OF EVENTS

All the film was scanned once and approximately three-fourths of it was re-scanned. The topologies used in this analysis were two-pronged events with either one or two visible neutral V's. Events were measured with either Franckenstein or Vanguard measuring machines and fitted using the two-view reconstruction and fitting program PACKAGE. A small sub-sample of events was also processed with the three view TVGP-SQUAW program to check for possible biases in the fitting procedure. The identification of events in the two cases was invariably the same.

Examples of the reaction $pp \rightarrow \Sigma^0 pK^0\pi^+$ were not included in the analysis because of the small number of events and rather serious biases. A fit to either b) or c) was accepted if the V^0 fitted the 3c Λ hypothesis and if the 1c fit for the production hypothesis had a χ^2 less than 5.0. For reaction a), events with two visible V^0 decays were accepted if the corresponding 4c fit to the production hypothesis had a confidence level greater than 0.005. In all cases, the predicted bubble densities for the two charged tracks at the production vertex were required to be compatible with those observed. Events which, after repeated measurement, failed to fit kinematics of one of the four-body reactions were considered to have two or more unobserved neutrals.

Except for a negligible number, all fitting ambiguities are among production hypotheses with the same observed neutral particle. Except for ambiguities between the 4c fit $\Lambda pK^0\pi^+$ and the 2c fit $\Sigma^0 pK^0\pi^+$, which are discussed below, events ambiguous among fits of different constraint class were assigned to the hypothesis of higher constraint.

Table I. Event totals and cross sections for pp four-body reactions containing a Λ.

Category	Observed No. of events	Corrected No.[A] of events	Cross section (μb)
$\Lambda pK^{o}\pi^{+}$	959	990	64 ± 6
$\Sigma^{o}pK^{o}\pi^{+}$	160	164	11 ± 2
$\Lambda pK^{+}\pi^{o}$	492	531	39 ± 6
$\Lambda nK^{+}\pi^{+}$	554	614	43 ± 4
$\Lambda pK^{o}\pi^{+}$-$\Sigma pK^{o}\pi^{+}$	59	42	
$\Lambda pK^{o}\pi^{+}$-$\Lambda pK^{+}\pi^{o}$	71	71	
$\Lambda pK^{o}\pi^{+}$-$\Lambda nK^{+}\pi^{+}$	41	36	
$\Lambda pK^{+}\pi^{o}$-$\Lambda K^{+}p\pi^{o}$	20	19	
$\Lambda nK^{+}\pi^{+}$-$\Lambda n\pi^{+}K^{+}$	50	55	
Λ + 2 prong + two or more missing neutrals	1148	1275	

A. These are the corrected numbers of events after minimum length and projected opening angle cuts and corresponding weightings have been applied to the data.

In Table I we give the observed number of events for each of the various categories.

III. CROSS SECTIONS

Corrections to the observed numbers of events were made to accomodate observational biases. The observed proper lifetime distributions for both Λ's and K^0's are depleted for times $t < 0.2\tau$, where τ is the mean life-time, because of low efficiency for detection of V^0 decays near the production vertex. A minimum decay length cutoff of 1.2 cm and a corresponding weighting were applied to the sample to correct for this effect. Evidence for bias against Λ's with small projected opening angle was found in the angular distribution of the lambda decay. We define ϕ to be the angle between the plane of the decay and a plane containing the Λ direction and a vector perpendicular to the plane of the chamber. Deviations from isotropy were observed in the distribution in ϕ, Fig. 1, indicating a bias against small projected opening angles. Only events with projected opening angle greater than three degrees were retained and weighted appropriately. The average weights for the length and projected opening angle corrections are 1.11 and 1.23 respectively. Table I gives the corrected number of events. Study of the K^0 decay distributions indicated an additional bias against detection of slow K^0's. Disagreement with the expected branching ratios of 1/4/2 for $(\Lambda)pK^0\pi^+/\Lambda p(K^0)\pi^+/\Lambda pK^0\pi^+$, where parentheses denote an unobserved neutral, reflects this bias. Reexamination of events which fit $pp \rightarrow \Lambda p(K^0)\pi^+$ with missing K^0 momentum less than 500 MeV/c revealed missed decays in the chamber volume. After correction,

the ratios of cross sections are satisfactory. Events were not weighted to correct for this bias since only 30 events were completely missing from the sample of 1000 events and no biases in effective mass distributions were indicated.

The center-of-mass reflection symmetry of proton-proton collisions was exploited to determine evidence for biases in the data. First, we present evidence in Fig. 2a that the criteria for the assignment of events to the category of two missing neutrals gives a sample consistent with center-of-mass symmetry. This shows the distribution in the cosine of the lambda production angle in the overall center of mass using weighted events. The reference direction is defined by the beam proton. About half of the entire sample of events are in this histogram. The normalized curve is a rough fit to the data and is included only to indicate agreement with symmetry. Figure 2b shows the production angular distribution for Λ's in all the identified final states. Events of the channel $\Lambda n K^+ \pi^+$ show the greatest departure from reflection symmetry, as seen in the Λ production angular distribution of Fig. 2c. A scatter plot of $\cos \theta_\Lambda$ vs $\cos \theta_n$, where θ_Λ, θ_n are the center-of-mass production angles with respect to the beam proton, shows 730 events with Λ and n in opposite hemispheres. Of these, 360 have $\cos \theta_\Lambda > 0$, 370 have $\cos \theta_\Lambda < 0$, consistent with reflection symmetry. Of the 178 events with Λ and n in the same hemispheres, only 60 have the two baryons together in the forward hemisphere. This is essentially the complete observed asymmetry. A source of contamination is the five-body state $\Lambda p \pi^+ (K^0 \pi^0)$. About 150 examples of this reaction have been obtained with both K^0 and Λ decays observed. The fraction of these events which

fitted the $\Lambda(n)K^+\pi^+$ hypothesis, after eliminating the K^0 decay measurement, and which were consistent with the bubble densities, indicates that the asymmetry can be solely accounted for by contamination from the channel $\Lambda p\pi^+(K^0\pi^0)$. Except for 3 of 27 events, this falsely identified sample populated only that quadrant having the event excess, i.e. that defined by $\cos\theta_n < 0$, $\cos\theta_\Lambda < 0$. These events showed no other significant deviations from the effective mass and angular distributions of the true events. Therefore, for the $\Lambda(n)K^+\pi^+$ final state, only the cross section was corrected. In addition to those five-body events which fitted the $\Lambda nK^+\pi^+$ hypothesis after removal of the K^0, a smaller number fitted the $\Lambda pK^+\pi^0$ hypothesis. This sample was statistically insufficient for studying differential biases. Besides this source and the $pp \to \Sigma^0 pK^+$ events ambiguous with the hypothesis $\Lambda pK^+\pi^0$, we expect the $\Lambda pK^+\pi^0$ and the $\Lambda nK^+\pi^+$ events to be contaminated by four-body final states with Σ^0's. Unfortunately cross sections for $pp \to \Sigma^0 pK^+\pi^-$, $\Sigma^0 nK^+\pi^+$ are unknown so the magnitude of this contamination cannot be determined. With the assumption that the relative production rate of Σ^0 and Λ for each of these two four-body K^+ states is the same as in the final states $\Sigma^0 pK^0\pi^+$ and $\Lambda pK^0\pi^+$ and that their production mechanisms are similar, the Σ^0 contamination in these K^+ states is expected to be less than 8%. This number is based on the assumption that all of the ambiguities between $\Lambda pK^0\pi^+$ and $\Sigma^0 pK^0\pi^+$ belong to the latter category, and is hence likely to be an over-estimate. In fact, judging from the center-of-mass angular distribution for $\Lambda pK^0\pi^+$ production it is probable that most of those events are truly Λ events. We

have shown in a previous article[4] that this is the case for ΛpK^+ - $\Sigma^o pK^+$ ambiguous events. Events ambiguous between two kinematic hypotheses are included in both categories with a weighting factor of 1/2. No significant changes in mass and angular distributions are observed when this factor is varied from 0 to 1. The biases we have discussed contribute relatively small numbers of events compared to the totals.

Beam tracks were counted in 1,000 frames evenly spaced throughout the film yielding 5,090,000 ± 150,000 for the total number of noninteracting protons. The uncertainty given is not the statistical error but rather the average deviation of several measurements. Using a fiducial length of 125 cm., total p-p interaction cross section 40.6 mb,[10] and target proton density of $(0.361 \pm 0.007)\ 10^{23}/cm^3$, we obtain $\sigma_i = N_i(0.0401 \pm 0.0014)\mu b$ as the partial cross section for channel i. N_i is the sum of the weights for the events in the channel and the uncertainty in N_i is

$$\sqrt{\sum_j w_j^2}$$

where w_j is the weight for the j^{th} event. In making the path length determination, we have used 1.6 mb[11] as the cross section for unobserved low momentum transfer elastic scatters. Comparing two independent scans, an efficiency of 0.96 ± 0.02 was found. The production cross sections obtained for the various final states are given in Table I.

IV. RESONANCE PRODUCTION

Since the three final states $\Lambda pK^o\pi^+$, $\Lambda pK^+\pi^o$, and $\Lambda nK^+\pi^+$ each

contain the same hadrons differing only in their charges, we expect the dynamical mechanisms of their production to be related. With few exceptions, we indeed find the same general behavior in the data for each state. Therefore, we discuss the three final states simultaneously.

In Figs. 3, 4, and 5 we display the various $N\pi$, $\Lambda\pi$, and $K\pi$ effective mass spectra. All the established pionic resonances, Y*(1385), K*(890), and N*(1236) are present. We find evidence in all channels for peripheral production of $N^*_{3/2}(1950)$ with subsequent decay into Y*K. Analysis of this reaction has been presented elsewhere.[9]

In order to estimate the relative production rates of the pionic resonances, we have fitted the data for each final state to a sum of pure phase space plus resonance production. Although certain features of the data are certainly in disagreement with the simplifying assumptions of isotropic production and decay of the resonances, we nevertheless are able to estimate reliably the relative cross sections for N*, K*, and Y* production.

In four-body production where no correlation of the final state with the initial state is included, five independent variables are necessary to specify the final state. For each final state the experimental density was fitted to a function of the five kinematic variables, consisting of an incoherent sum of terms representing resonant processes and phase space,

$$f(x) = \sum_{j=1}^{N} \alpha_j |M_j(x)|^2 \rho(x) \quad .$$

The α_j are the relative intensities of the different processes, x denotes the set of five independent variables, the $|M_j|^2$ are proportional to the corresponding Lorentz invariant matrix elements squared and $\rho(x)$ is the phase space density. The normalization conditions are:

$$\int |M_j(x)|^2 \rho(x) dx_1 .. dx_5 = 1 \text{ for each } j$$

and

$$\sum_{j=1}^{N} \alpha_j = 1 \quad .$$

The α_j were determined by a maximum-likelihood method.

For the N*(1236), K*(890), and Y*(1385) resonance terms we use

$$|M_j|^2 = \text{const} \frac{m^2}{p} \frac{\Gamma(m)}{(m^2-m_o^2)^2 + m_o^2 \Gamma^2(m)}$$

where m is the invariant mass of the resonant pair of particles and p is the momentum of either one in the rest frame of m. The total width is used both in the denominator and numerator since all the resonances are nearly elastic. The constants are determined by the normalization conditions above. For N*(1236) and Y*(1385) we use:

$$\frac{\Gamma(m)}{\Gamma(m_o)} = \left(\frac{p}{p_o}\right)^3 \left(\frac{m_o}{m}\right) \frac{(E_B+m_B)}{(E_B^o+m_B)}$$

where E_B is the energy of the baryon in the resonance rest system, m_B is the mass of the baryon and p_o and E_B^o are the values of p and E_B at the nominal resonance mass, m_o. For K*(890) we use

$$\frac{\Gamma(m)}{\Gamma(m_o)} = \left(\frac{p}{p_o}\right)^3 \left(\frac{m_o}{m}\right)^2 \quad .$$

Table II gives the results of fits for the relative intensities and corresponding cross sections. The errors quoted are estimates of the precision with which we determine the various relative intensities. The resonance cross sections are seen to be in reasonable agreement with charge-independence requirements, which predict ratios of 9/2/1 for $\Lambda K^0(N^{*++} \rightarrow p\pi^+)/\Lambda K^+(N^{*+} \rightarrow p\pi^0)/\Lambda K^+(N^{*+} \rightarrow n\pi^+)$ and 2/1 for $(K^{*+} \rightarrow K^0\pi^+)/(K^{*+} \rightarrow K^+\pi^0)$. The curves superimposed on the experimental histograms of Figs. 3, 4, and 5 show the mass distributions obtained with this model. Except for the $K^0\pi^+$ and $K^+\pi$ mass distributions, the agreement is excellent. The enhancements seen in the low $(K\pi)^+$ mass region correspond to a mass of 725 MeV/c^2 and a width of 70 MeV/c^2. There have been similar observations in different experiments, but interpretation of them as evidence for a resonance has been generally unconvincing because of inconsistencies in production rates and observed widths.[12] It is possible that the effects are dynamically correlated with N*(1236) or Y*(1385) production. Lack of an enhancement in the $K^+\pi^+$ mass distribution for the $\Lambda K^+\pi^+$ state, where Y*(1385) production is strongest, tends to rule out Y*(1385) as a source. It may be important that the $K\pi$ enhancement is largest in the state where N*(1236) production is dominant and absent in the state where no N*(1236) is observed. Of course, a K-π interaction in I = 1/2 only, would also account for this observation. In the corresponding predictions of pion-exchange model discussed below, the $K^0\pi^+$ mass distribution (displayed in Fig. 12 f) fails to indicate any peaking in the low $K\pi$ mass region.

The $K\pi$, $N\pi$, and $\Lambda\pi$ effective mass distributions are in rather good agreement with the above model. Since we assume isotropic production

Table II. Resonance cross sections for $pp \rightarrow \Lambda NK\pi$ at 6 BeV/c.

	Y*(1385)	N*(1236)	K*(890)	Background
$\Lambda pK^0\pi^+$				
Relative Fraction	0.18±0.02	0.36±0.04	0.10±0.03	0.36±0.04
Cross section (μb)	11±2	23±3	6±2	23±3
$\Lambda pK^+\pi^0$				
Relative Fraction	0.19±0.03	0.10±0.04	0.04±0.02	0.67±0.04
Cross section (μb)	7±1	4±2	2±1	26±4
$\Lambda nK^+\pi^+$				
Relative Fraction	0.34±0.02	0.0 ±0.03	--	0.66±0.03
Cross section (μb)	15±2	0±1	--	29±3

and decay of resonances we expect angular distributions and some effective mass distributions not to agree with the model. The ΛN mass distributions are in gross disagreement; for example Fig. 6 gives the Λp mass distribution for the $\Lambda p K^0 \pi^+$ final state.

V. ONE-PION EXCHANGE

Those features of the data which are sensitive to the production and decay angular distributions of the resonances can be included in the framework of a single particle exchange model. Although several particle exchange processes can contribute to the amplitude for each reaction, we make the assumption that only pion exchange is present and do not consider other processes such as kaon exchange. We have shown in an earlier paper that pion exchange alone is a good description for three body strange particle final states. The exchange model is found to give a satisfactory description of the present data as well.

Fig. 7 shows the possible single pion exchange diagrams. The diagram of Fig. 7a requires fewest assumptions for the calculation since the vertices involve only two-body scattering processes. The Nπ cross sections are known very well and the ΛK cross section has been fairly well studied. The amplitude of diagram 7b can be separated into contributions from Figs. 7c, d, e assuming that the only resonances produced are K*(890) and Y*(1385). The cross section for a final state is then calculated as an incoherent sum of squares of the corresponding amplitudes for the four diagrams (a), (c), (d), and (e). Contribution to the amplitude from the diagram obtained by interchange

of the two initial state protons is included. This gives just a factor of two in the cross section with neglect of interference terms, justified by the strongly peripheral character of the reactions.

For the calculation of the diagram 7(a) we follow Salzman and Salzman[13] and assume that both virtual pion interactions can be represented by the real pion cross sections at the same total energy. The differential cross section is then

$$\frac{d^7\sigma}{dm^2_{N\pi}dm^2_{\Lambda K}dtd\cos\theta_{N\pi}d\phi_{N\pi}d\cos\theta_{\Lambda K}d\phi_{\Lambda K}} = \frac{1}{32\pi^3}\frac{1}{(\bar{p}\bar{E})^2}\frac{1}{(t+\mu^2)^2}\frac{d\sigma_{N\pi}}{d\Omega_{N\pi}}\, k_{N\pi}m_{N\pi} \cdot \frac{d\sigma_{\Lambda K}}{d\Omega_{\Lambda K}}\, k_{\Lambda K}m_{\Lambda K} \cdot$$

Here

$m_{N\pi}$ and $m_{\Lambda K}$ are the effective masses of the pairs of particles.

t is the square of the four-momentum transfer between the initial proton and the $N\pi$ system.

$\theta_{N\pi}$ is the angle between the initial proton and the final state nucleon in the $N\pi$ rest system and

$\phi_{N\pi}$ is the corresponding azimuthal angle of the nucleon about the initial proton direction.

$\theta_{\Lambda K}$ and $\phi_{\Lambda K}$ are defined analogously to $\theta_{N\pi}$ and $\phi_{N\pi}$.

$\bar{p}$ and $\bar{E}$ are the momentum and energy of either initial state proton in the overall center of mass.

$\frac{d\sigma_{N\pi}}{d\Omega_{N\pi}}$ and $\frac{d\sigma_{\Lambda K}}{d\Omega_{\Lambda K}}$ are the experimental differential cross sections for $\pi p \to N\pi$ and $\pi p \to \Lambda K$ respectively.

$k_{N\pi}$ and $k_{\Lambda K}$ are the momenta of real pions in the center of mass for the reactions $\pi p \to N\pi$ and $\pi p \to \Lambda K$ at total energies $m_{N\pi}$

and $m_{\Lambda K}$ respectively.

The experimental $\pi p \to \pi N$ cross sections were calculated from a recent phase shift analysis.[14] In the energy range needed for our four-body states, these cross sections are dominated by N*(1236) production. The various $\pi p \to \Lambda K$ differential cross sections we use are taken from reports listed in reference 15.

For the process describing Y*(1385) production we use

$$\frac{d^7\sigma}{dm^2_{\Lambda\pi}\,dw^2\,dt\,d\cos\theta_{\Lambda\pi}\,d\phi_{\Lambda\pi}\,d\cos\theta_{\Lambda}\,d\Phi_{\Lambda}} =$$

$$\frac{G^2}{4\pi}\,\frac{1}{16\pi}\,\frac{e^{-\alpha(t+m_\pi^2)}\,t}{(t+m_\pi^2)^2}\,\frac{1}{(\bar{p}\bar{E})^2}\,kw\,\frac{d\sigma_{Y^*}}{d\Omega}\,(w,\theta_{\Lambda\pi})\,\frac{p_\Lambda}{m_{\Lambda\pi}}\,\frac{p_{\Lambda\pi}}{(m^2_{\Lambda\pi}-m_o^2)^2+m_o^2\Gamma^2}\cdot y(w)$$

where

$$\frac{1}{y(w)} = \int_{(m_\Lambda+m_\pi)^2}^{(w-m_k)^2} \frac{4\pi\, p_{\Lambda\pi}\, p_\Lambda}{m_{\Lambda\pi}[(m^2_{\Lambda\pi}-m_o^2)^2+m_o^2\Gamma^2]}\,dm^2_{\Lambda\pi}$$

$\frac{G^2}{4\pi}$ = 15 for π^o exchange, = 30 for π^+ exchange.

w is the effective mass of $\Lambda K\pi$ system.

k is the c.m. momentum of a real pion in the initial state for $\pi p \to \Lambda K\pi$ at total energy w.

t is the square of the four-momentum transfer between initial state proton and final state nucleon.

$\theta_{\Lambda\pi}$ and $\phi_{\Lambda\pi}$ are the angles describing the $\Lambda\pi$ system defined in the $\Lambda K\pi$ rest system.

θ_Λ and ϕ_Λ are the angles describing the Λ in the $\Lambda\pi$ rest system.

$\frac{d\sigma_{Y^*}}{d\Omega}(w,\theta_{\Lambda\pi})$ is the differential cross section for Y*(1385) production at total energy w.

$p_{\Lambda\pi}$ is the momentum of the $\Lambda\pi$ system in the $\Lambda K\pi$ rest system.

p_{Λ} is the momentum of the Λ in the $\Lambda\pi$ rest system.

m_0 and Γ_0 = 1.385 BeV/c^2 and 0.040 BeV/c^2, respectively.

The factor $e^{-\alpha(t+m_\pi^2)}$ was included to obtain agreement with the four-momentum transfer distribution in the $nY^{*+}K^+$ final state. We find $\alpha = 1.0$ (BeV/c)$^{-2}$ adequate for all three final states.

The momentum dependence for the Y* decay could also include a p wave decay factor but since the Y* is narrow the results are not sensitive to this factor.

Similar expressions are used to describe K*(890) production, with resonance parameters m_0 = 890 MeV/c^2, Γ_0 = 50 MeV/c^2. The factor $e^{-\alpha(t+m_\pi^2)}$ is omitted as unnecessary for a good fit to the data.

To describe the non-resonant background, we assume $\pi p \to \Lambda K\pi$ to be described by pure phase space. This assumption is clearly not valid at high values of $\Lambda K\pi$ mass and neglects the low mass ΛK interaction which is probably present. The background cross section we use is then

$$\frac{d^7\sigma}{dm_{\Lambda\pi}^2 dw^2 dt d\cos\theta_{\Lambda\pi} d\phi_{\Lambda\pi} d\cos\theta_\Lambda d\phi_\Lambda} = \frac{G^2}{4\pi}\frac{1}{16\pi}\frac{t}{(t+m_\pi^2)^2}\frac{1}{(\bar{p}\bar{E})^2} kw\sigma(w) p_{\Lambda\pi}\frac{p_\Lambda}{m_{\Lambda\pi}} A(w)$$

where

$$\frac{1}{A(w)} = 16\pi^2 \int_{(m_\Lambda+m_\pi)^2}^{(w-m_K)^2} \frac{p_{\Lambda\pi}\, p_\Lambda}{m_{\Lambda\pi}}\, dm_{\Lambda\pi}^2$$

$\sigma(w)$ is the $\pi p \to \Lambda K\pi$ cross section at total energy w. The other definitions are the same as before.

The energy dependence of the total cross section for $\pi^0 p \to Y^{*+}K^0$, $\pi^0 p \to Y^{*0}K^+$, and $\pi^0 p \to \Lambda K^{*+}$, as well as their angular distributions, are needed for the calculation of production cross sections for the states $\Lambda p K^0 \pi^+$ and $\Lambda p K^+ \pi^0$. In addition, $\pi^+ p \to Y^{*+}K^+$ data are required to calculate the $\Lambda n K^+ \pi^+$ rate. The π^0 cross sections were obtained from the following isotopic spin relations:

$$\sigma(\pi^0 p \to \Lambda K^0 \pi^+) = \sigma(\pi^- p \to \Lambda K^0 \pi^0)$$

and

$$\sigma(\pi^0 p \to \Lambda K^+ \pi^0) = 1/2[\sigma(\pi^+ p \to \Lambda K^+ \pi^+) + \sigma(\pi^- p \to \Lambda K^+ \pi^-) - \sigma(\pi^- p \to \Lambda K^0 \pi^0)].$$

The available data are shown in Figs. 8, 9, 10, and 11. The smooth curves drawn through the measured values of total cross sections are qualitative representations of the variation with energy. They provide interpolated values of cross sections used in the pion-exchange calculation. Using the experimental data of Fig. 11 for $\pi^- p \to \Lambda K^{*0}$ and charge independence requirements, the K* production cross sections of Figs. 8 and 9 were determined. The curves of Y* production cross section are somewhat crude fits to the sparse available experimental data and the background curves were obtained by subtraction. No $\pi^- p \to Y^{*0}K^0$ production angular distributions are available in the literature. Therefore, we have used angular distributions derived from the present data for Y* production. For K*(890) production, experimental differential production cross sections are used.

We have fitted the data for each final state to the predictions of the single pion exchange model. The relative intensities obtained for the different processes are in excellent agreement with those found in the fit described in Section IV. The calculated cross sections given

in Table III are not in agreement with our measured cross sections. Since one can introduce form factors which do not significantly alter the shapes of distributions, but result in rather different total cross sections, we do not take this discrepancy as evidence of failure of the model.

We compare our experimental distributions with the pion exchange model. All calculations of experimental quantities, such as scattering angles, which require specification of an initial state proton were made by associating with any final system that proton with the smallest momentum transfer to the system. This same selection was included in the Monte Carlo calculations. We find less than 15% of the Monte Carlo events required interchange of initial state protons for the calculation of distributions. In Figs. 12, a through j, we display the six two-body and the four three-body effective mass distributions for $\Lambda p K^0 \pi^+$. We find similar agreement for the other channels not shown. In all the histograms we include the pion-exchange prediction with each contribution separately indicated.

We will discuss only the $\Lambda p K^0 \pi^+$ final state since agreement with the model is somewhat better than for the other channels and the input data is of higher quality. This is the channel with the largest number of events and least contamination. As discussed above, the low $K^0 \pi^+$ effective mass region is not fit well by the model. The fit to the $p\pi^+$ effective mass, shown in Fig. 12e has been shown to be improved by inclusion of off-mass-shell corrections, such as those of Dürr and Pilkuhn.[16] These tend to shift the resonance peak to a slightly lower value and result also in a somewhat narrower effective width for the

Table III. One-pion exchange predicted cross sections for $pp \rightarrow \Lambda NK\pi$ at 6 BeV/c.

	Y*(1385)	N*(1236)	K*(890)	Background
$\Lambda pK^0\pi^+$	15 μb (with form factor) 41 μb (no form factor)	21 μb	28 μb	34 μb
$\Lambda pK^+\pi^0$	8 μb (with form factor) 22 μb (no form factor)	6 μb	14 μb	20 μb
$\Lambda nK^+\pi^+$	48 μb (with form factor) 130 μb (no form factor)	3 μb		46 μb

resonance.

Further, more critical tests of the adequacy of the one-meson-exchange model were made by comparing angular distributions with predictions. This is a sensible procedure only if there exist reasonably accurate on-mass-shell pion reaction data. As discussed above, this is true only for the $\Lambda p K^0 \pi^+$ state. In Figs. 13 and 14 we plot the angular distribution of the proton in the $p\pi^+$ rest system and the Λ in the ΛK^0 rest system. The reference direction in both cases is the momentum transfer to the two-body system. Satisfactory agreement is obtained. Thus the off-mass-shell scattering and production angular distributions are well represented by on-mass-shell experimental data.

Another test of the model is the Treiman-Yang angular distributions. We compute the angle between the normal to the plane containing the K momentum and momentum transfer in the $\Lambda K\pi$ center of mass and the normal to the plane of the incident and recoil nucleons. This angle has the meaning of the usual Treiman-Yang angle for those events which are produced by the exchange diagram 7b and so has a simple distribution for those events not containing N*. All events are included in the distributions shown in Fig. 15. The curves shown include the effects of diagram 7a, i.e. they include the distribution in this angle for events containing N*(1236) as well. Comparison with theory of the Treiman-Yang distribution for all events is therefore a test of the entire model. Again agreement with the model is quite good. Finally, in Fig. 16 we show the distribution in momentum transfer to the final state proton for all events identified as $\Lambda p K^0 \pi^+$. The data are well

fit by the model over the complete range of momentum transfer. Similar results are observed in the other final states supporting the conclusion that the data are well represented by the one-pion exchange model.

CONCLUSIONS

Resonance production via quasi-two-body and three-body channels contribute strongly to strange particle production in four-body final states. A simple one-pion exchange mechanism including empirical form factors gives predictions in good agreement with the data.

REFERENCES

1. Results on production of N* resonances in pp collisions, using missing-mass spectrometer techniques, are reported in:
K. J. Foley, R. S. Jones, S. J. Lindenbaum, W. A. Love, S. Ozaki, E. D. Platner, C. A. Quarles, and E. H. Willen, Phys. Rev. Letters 19, 397 (1967).
I. M. Blair, A. E. Taylor, W. S. Chapman, P. I. P. Kalmus, J. Litt, M. C. Miller, D. B. Scott, H. J. Sherman, A. Astbury, and T. J. Walker, Phys. Rev. Letters 17, 789 (1966).
E. W. Anderson, E. J. Bleser, G. B. Collins, T. Fujii, J. Menes, F. Turkot, R. A. Carrigan, Jr., R. M. Edelstein, N. C. Hien, T. J. McMahon, and I. Nadelhaft, Phys. Rev. Letters 16, 855 (1966).
C. M. Ankenbrandt, A. R. Clyde, B. Cork, D. Keefe, L. T. Kerth, W. M. Layson, and W. A. Wenzel, Nuovo Cimento 35, 1052 (1965).
G. Cocconi, E. Lillethun, J. P. Scanlon, C. A. Stahlbrandt, C. C. Ting, J. Walters, and A. M. Wetherell, Phys. Letters 8, 134 (1964).
G. G. Chadwick, G. B. Collins, P. J. Duke, T. Fujii, N. C. Hien, M. A. R. Kemp, and F. Turkot, Phys. Rev. 128, 1823 (1962).
G. Cocconi, A. N. Diddens, E. Lillethun, G. Manning, A. E. Taylor, T. G. Walker, and A. M. Wetherell, Phys. Rev. Letters 7, 450 (1961).

Results on pion production in pp collisions are contained in:
D. V. Bugg, A. J. Oxley, J. A. Zoll, J. G. Rushbrooke, V. E. Barnes, J. B. Kinson, W. P. Dodd, G. A. Doran, and L. Riddiford, Phys. Rev. 133, B1017 (1964).

A. P. Colleraine and U. Nauenberg, Phys. Rev. 161, 1387 (1967).

S. Coletti, J. Kidd, L. Mandelli, V. Pelosi, S. Ratti, V. Russo, L. Tallone, E. Zampieri, C. Caso, F. Conte, M. Dameri, C. Grosso, and G. Tomasini, Nuovo Cimento 49A, 479 (1967).

A. M. Eisner, E. L. Hart, R. I. Louttit, and T. W. Morris, Phys. Rev. 138, B670 (1965).

E. L. Hart, R. I. Louttit, D. Luers, T. W. Morris, W. J. Willis, S. S. Yamamoto, Phys. Rev. 126, 747 (1962).

W. J. Fickinger, E. Pickup, D. K. Robinson, and E. O. Salant, Phys. Rev. 125, 2082 (1962).

E. Pickup, D. K. Robinson, and E. O. Salant, Phys. Rev. 125, 2091 (1962).

G. A. Smith, H. Courant, E. C. Fowler, H. Kraybill, J. Sandweiss, and H. Taft, Phys. Rev. 123, 2160 (1961).

Robert Ronald Kinsey, "Zero Strangeness Resonance Production in 6 GeV/c Proton-Proton Collisions," (Ph.D. Thesis), University of California Lawrence Radiation Laboratory Report UCRL-17707, March 1968.

E. Gellert, G. A. Smith, S. Wojcicki, E. Colton, P. E. Schlein, and H. K. Ticho, Phys. Rev. Letters 17, 884 (1966).

E. Colton, P. E. Schlein, E. Gellert and G. A. Smith, Phys. Rev. Letters 21, 1548 (1968).

See also Ref. 2 below.

2. G. Alexander, O. Benary, G. Czapek, B. Haber, N. Kidron, B. Reuter, A. Shapira, E. Simopoulou, and G. Yekutieli, Phys. Rev. 154, 1284 (1967).

3. G. Alexander, A. Shapira, E. Simopoulou, and G. Yekutieli, Nuovo Cimento 53A, 455 (Jan. 1968).

4. W. Chinowsky, R. R. Kinsey, S. L. Klein, M. Mandelkern, J. Schultz, F. Martin, M. L. Perl, and T. H. Tan, Phys. Rev. 165, 1466 (1968).

5. E. Bierman, A. P. Colleraine, and U. Nauenberg, Phys. Rev. 147, 922 (1966).

6. W. M. Dunwoodie, H. K. Ticho, G. A. Smith, and A. B. Wicklund, UCLA-1031.

7. M. Firebaugh, G. Ascoli, E. L. Goldwasser, R. D. Sard, and J. Wray, Phys. Rev. 172, 1354 (1968).

8. T. Yao, Phys. Rev. 125, 1048 (1962).

9. W. Chinowsky, P. Condon, R. R. Kinsey, S. Klein, M. Mandelkern, P. Schmidt, J. Schultz, F. Martin, M. L. Perl, and T. H. Tan, Phys. Rev. 171, 1421 (1968).

10. R. F. George, K. F. Riley, R. J. Tapper, D. V. Bugg, D. C. Salter, and G. H. Stafford, Phys. Rev. Letters 15, 214 (1965).

11. A. R. Clyde (Ph.D. Thesis) UCRL-16275.

12. N. Barash-Schmidt, A. Barbaro-Galtieri, L. R. Price, A. H. Rosenfeld, P. Söding, C. G. Wohl, M. Roots, and G. Conforto, Rev. Mod. Phys. 41, 109 (1969).

13. F. Salzman and G. Salzman, Phys. Rev. 121, 1541 (1961).

14. A. Donnachie, R. G. Kirsopp, and C. Lovelace, Phys. Letters 26B, 161 (1968).

15. L. Bertanza, P. L. Connolly, B. B. Culwick, F. R. Eisler, T. Morris, R. Palmer, A. Prodell, and N. P. Samios, Phys. Rev. Letters 8, 332 (1962); J. Keren, Phys. Rev. 133, B457 (1964); J. A. Anderson,

Ph.D. Thesis University of California Radiation Laboratory Report No. UCRL-10838 (unpublished); F. Eisler, R. Plano, A. Prodell, N. Samios, M. Schwartz, J. Steinberger, P. Bassi, V. Borelli, G. Puppi, G. Tanaka, P. Woloscjek, V. Zobolli, M. Conversi, P. Franzini, I. Mannelli, R. Santangelo, and V. Silvestrini, Phys. Rev. 108, 1353 (1957); O. I. Dahl, L. M. Hardy, R. I. Hess, J. Kirz, D. H. Miller, and J. A. Schwartz, ibid. 163, 1430 (1967).

16. H. P. Dürr and H. Pilkuhn, Nuovo Cimento 40, 899 (1965).

FIGURE CAPTIONS

Fig. 1. Azimuth angle distribution of the decay proton for all Λ's with path length greater than 1.2 cm.

Fig. 2. Production angular distribution in the p-p center-of-mass for (a) events with two or more missing neutral particles, (b) all four-body events with a visible Λ and (c) events identified as $pp \rightarrow \Lambda n K^+ \pi^+$.

Fig. 3. Square of the effective mass of the $N\pi$ combination for the final states (a) $\Lambda p K^0 \pi^+$ (1170 events), (b) $\Lambda p K^+ \pi^0$ (708 events), and (c) $\Lambda n K^+ \pi^+$ (791 events). The curves are the theoretical distributions calculated with the phase space plus resonance model described in the text.

Fig. 4. Square of the effective mass of the $\Lambda\pi$ combination for the final states (a) $\Lambda p K^0 \pi^+$, (b) $\Lambda p K^+ \pi^0$ and (c) $\Lambda n K^+ \pi^+$. The curves show theoretical distributions obtained with the phase space plus resonance model.

Fig. 5. Square of the effective mass of the $K\pi$ combination for the final states (a) $\Lambda p K^0 \pi^+$, (b) $\Lambda p K^+ \pi^0$ and (c) $\Lambda n K^+ \pi^+$. The curves show theoretical distributions obtained with the phase space plus resonance model.

Fig. 6. Effective mass of the Λp combination for the final state $\Lambda p K^0 \pi^+$. The distribution obtained with the phase space plus resonance model is shown in the smooth curve.

Fig. 7. One pion exchange diagrams used in the calculations.

Fig. 8. Cross sections for $\pi^- p \rightarrow \Lambda K^+ \pi^-$ as a function of incident pion lab momentum. Experimental values of total cross sections and

Y* production are shown. The smooth curves are described in the text.

Fig. 9. Cross sections for $\pi^- p \to \Lambda K^0 \pi^0$ as a function of incident pion lab. momentum. Experimental values of total cross sections and Y* production are shown. The smooth curves are described in the text.

Fig. 10. Cross sections for $\pi^+ p \to \Lambda K^+ \pi^+$ vs incident pion momentum. Boxes indicate measured total cross sections; inscribed triangles are measured Y* production cross sections. At the two lowest momenta, the data are reported to be completely $Y^* K^+$ production. The curves are described in the text.

Fig. 11. Total cross sections for $\pi^- p \to \Lambda^0 K^{*0}$ vs incident pion momentum. The interpolated curve is discussed in the text.

Fig. 12. Effective mass distributions for all two-body and three-body combinations in the final state $\Lambda p K^0 \pi^+$. The curves superimposed on the experimental histograms are pion-exchange model predictions, calculated with Monte Carlo methods.

Fig. 13. Angular distribution of the proton in the $p\pi^+$ rest system for the final state $\Lambda p K^0 \pi^+$. The angle θ_p is between the proton direction and the momentum transfer to the $p\pi^+$ system. The curves show pion-exchange predictions.

Fig. 14. Angular distribution of the Λ in the ΛK^0 rest system for the final state $\Lambda p K^0 \pi^+$. The angle θ_Λ is between the Λ direction and the momentum transfer to the ΛK^0 system.

Fig. 15. Distribution of the Treiman-Yang angle for examples of the reaction $pp \to \Lambda p K^0 \pi^+$. The angle Φ_{TY} is between the plane

containing the incident and final protons and a plane containing the K momentum and the momentum transfer to the $\Lambda K\pi$ system, calculated in the $\Lambda K\pi$ rest system. The curves show the pion-exchange model prediction.

Fig. 16. Distribution of square of four-momentum transfer to the proton in the reaction $pp \rightarrow \Lambda p K^0 \pi^+$. The curves show the pion-exchange model predictions.

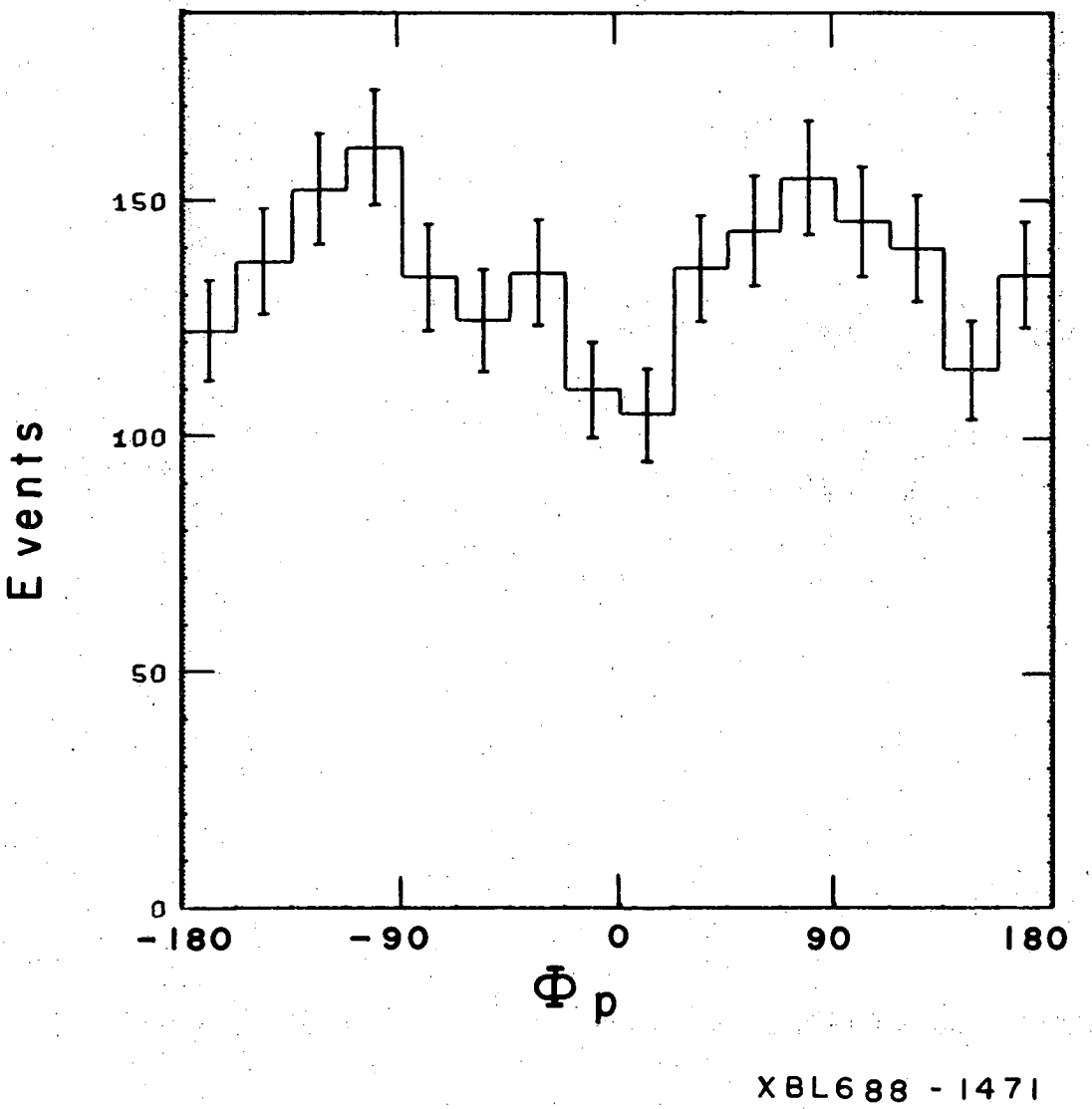

Fig. 1

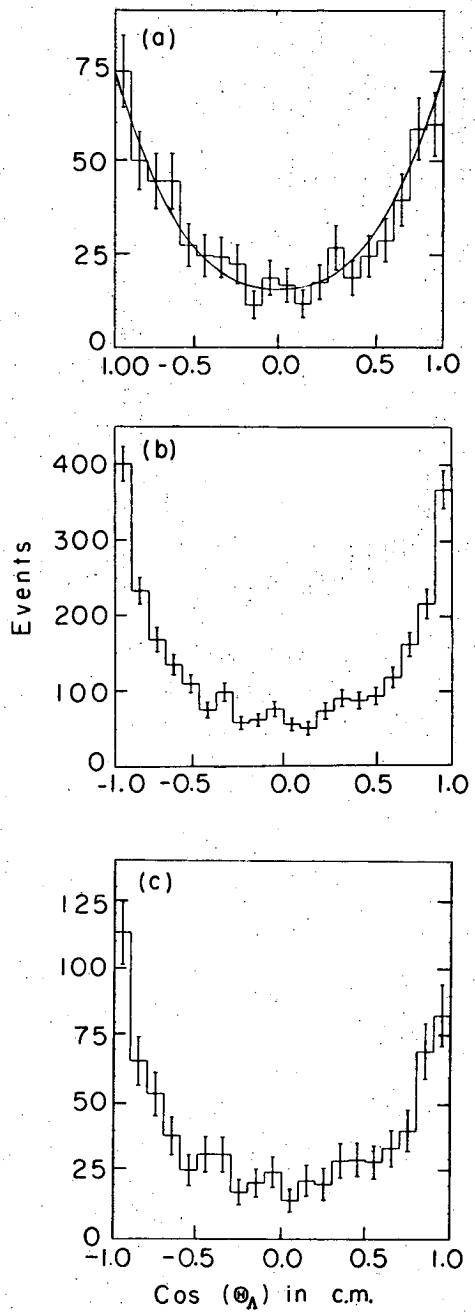

XBL6910-3920

Fig. 2

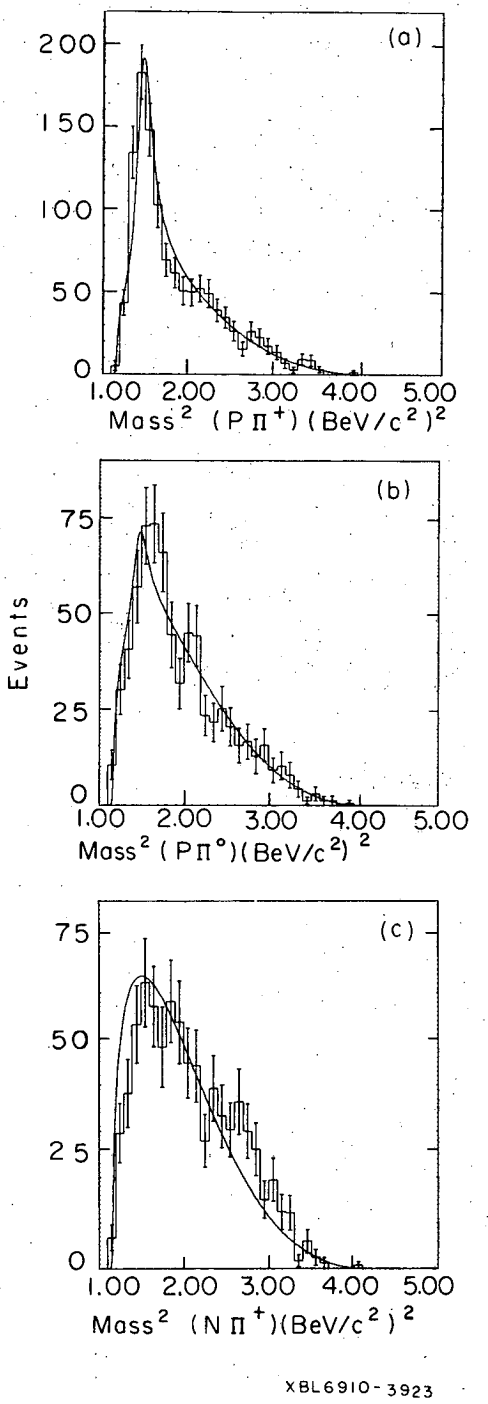
(a)
200
150
100
50
0
1.00 2.00 3.00 4.00 5.00
Mass^2 ($P\pi^+$) (BeV/c^2)^2
(b)
75
50
25
0
Events
1.00 2.00 3.00 4.00 5.00
Mass^2 ($P\pi^\circ$) (BeV/c^2)^2
(c)
75
50
25
0
1.00 2.00 3.00 4.00 5.00
Mass^2 ($N\pi^+$) (BeV/c^2)^2
XBL6910-3923

Fig. 3

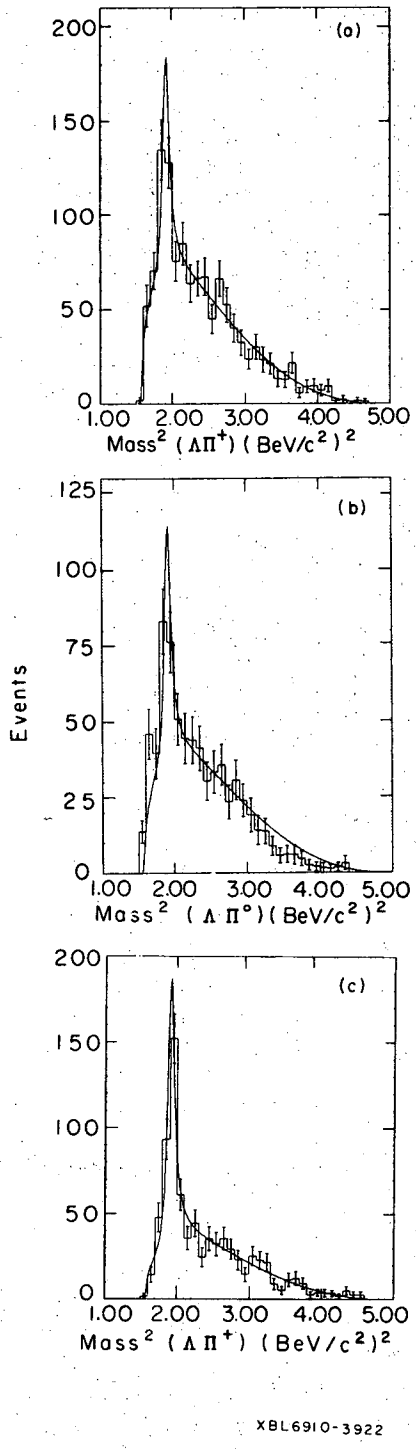
(a)
200
150
100
50
0
1.00 2.00 3.00 4.00 5.00
Mass^2 ($\Lambda\Pi^+$) (BeV/c^2)^2
(b)
125
100
75
50
25
0
Events
1.00 2.00 3.00 4.00 5.00
Mass^2 ($\Lambda\Pi^0$) (BeV/c^2)^2
(c)
200
150
100
50
0
1.00 2.00 3.00 4.00 5.00
Mass^2 ($\Lambda\Pi^+$) (BeV/c^2)^2
XBL6910-3922

Fig. 4

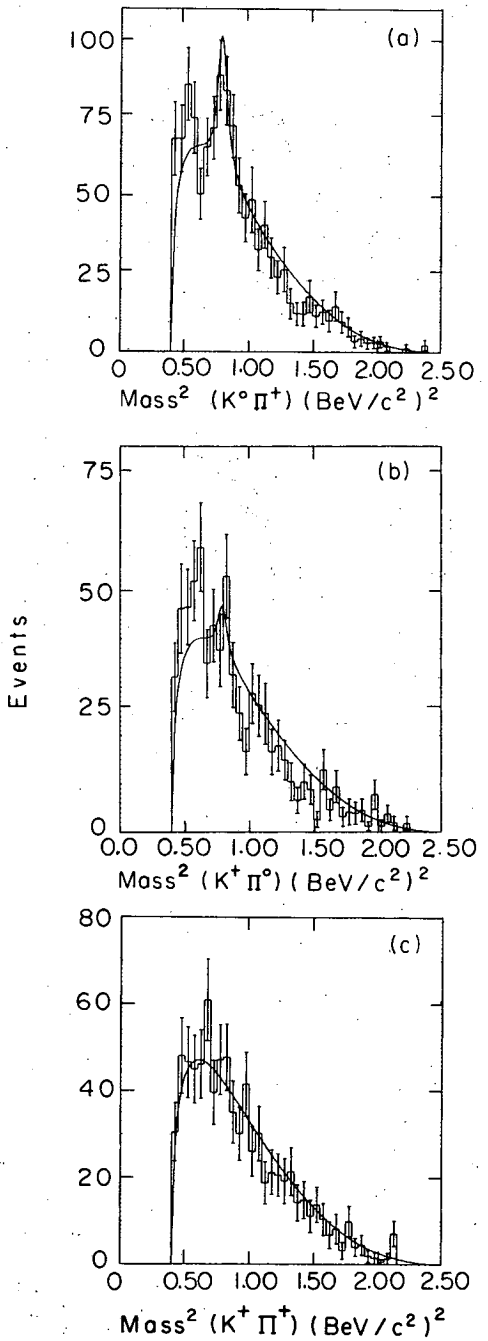
(a)
100
75
50
25
0
0 0.50 1.00 1.50 2.00 2.50
Mass² (K°π⁺) (BeV/c²)²
(b)
75
50
25
0
0.0 0.50 1.00 1.50 2.00 2.50
Mass² (K⁺π°) (BeV/c²)²
Events
(c)
80
60
40
20
0
0 0.50 1.00 1.50 2.00 2.50
Mass² (K⁺π⁺) (BeV/c²)²
XBL6910-3921

Fig. 5

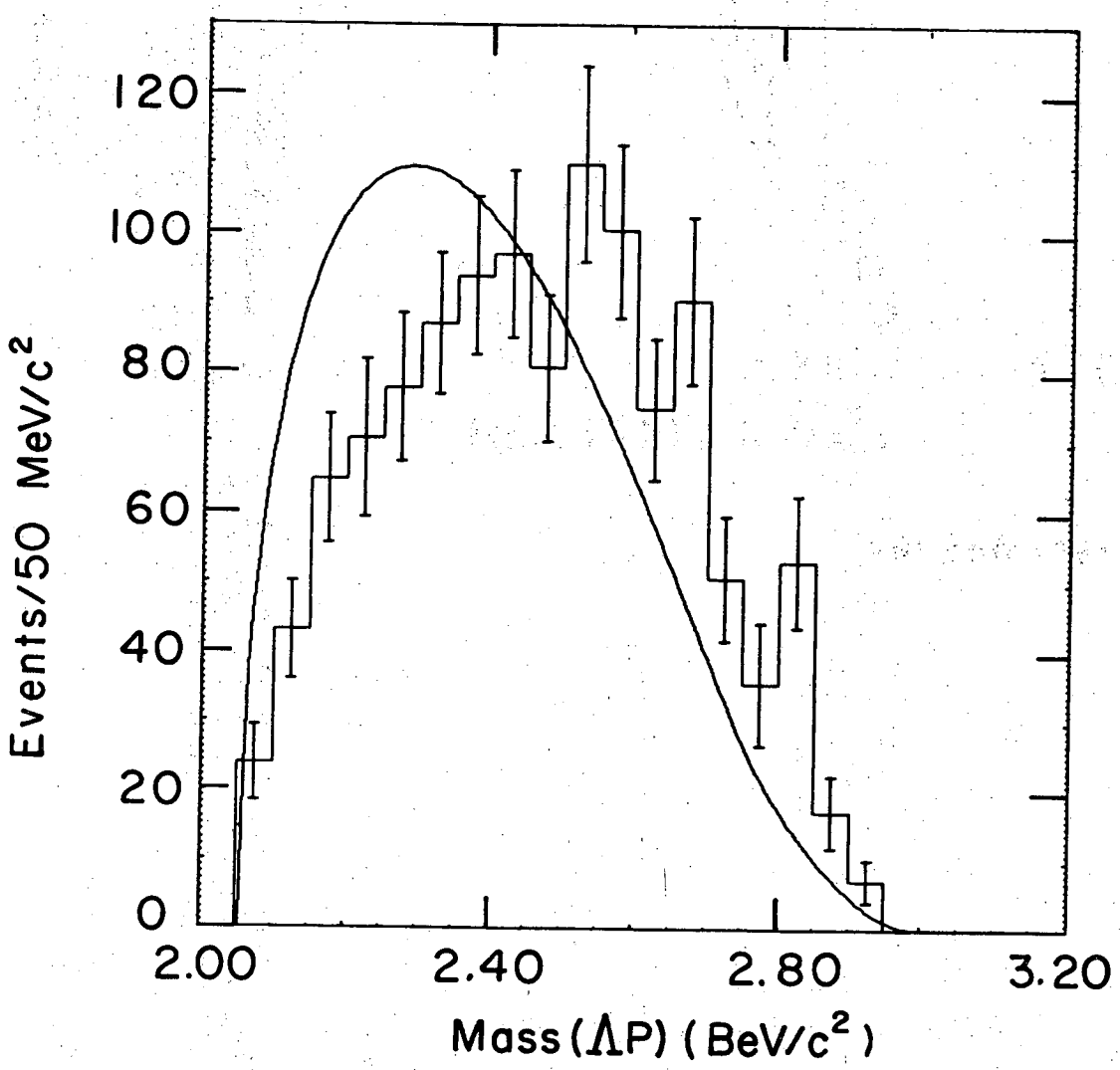

XBL688-1482

Fig. 6

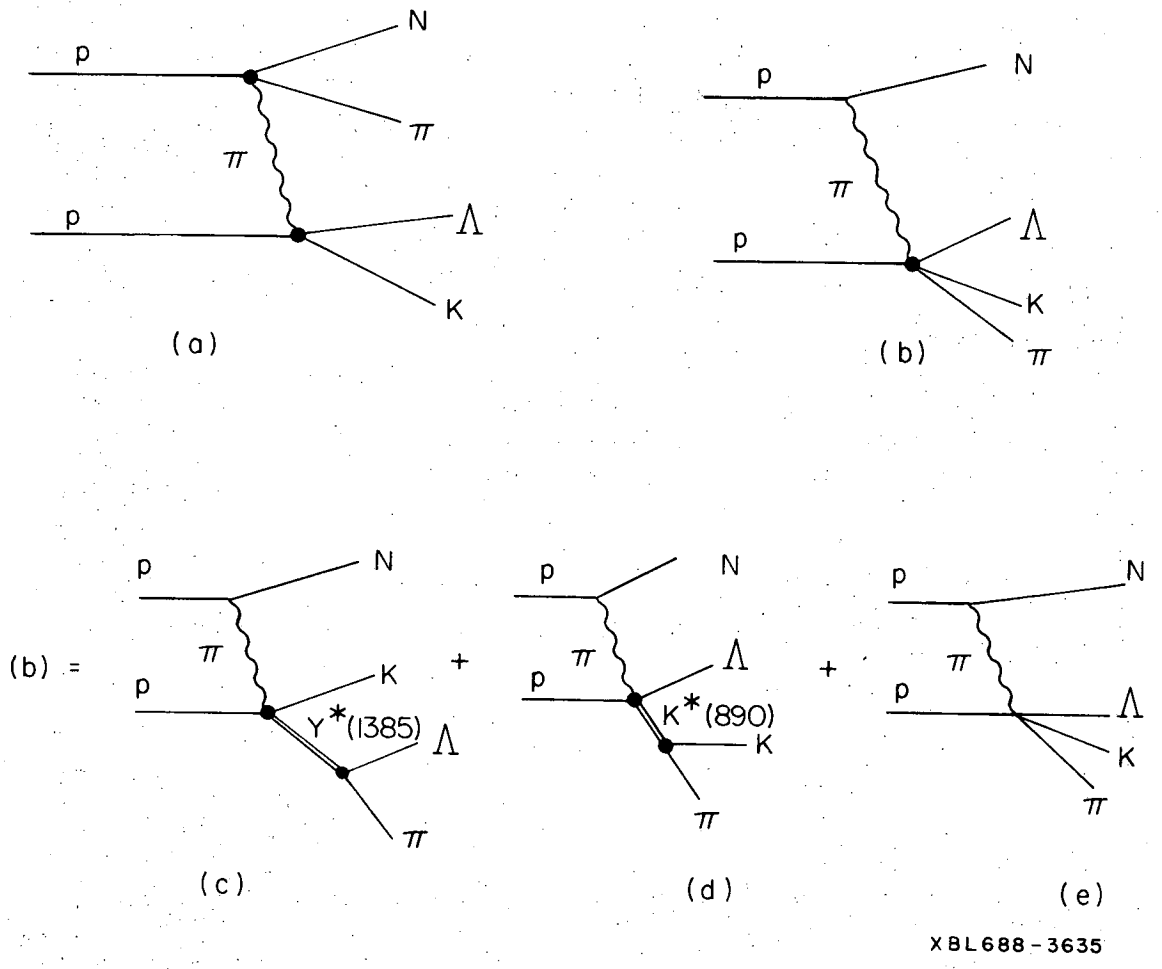
p
N
π
π
p
Λ
K
(a)
p
N
π
p
Λ
K
π
(b)
(b) =
p
N
π
K
p
Y*(1385)
Λ
π
(c)
+
p
N
π
Λ
p
K*(890)
K
π
(d)
+
p
N
π
p
Λ
K
π
(e)
XBL688-3635

Fig. 7

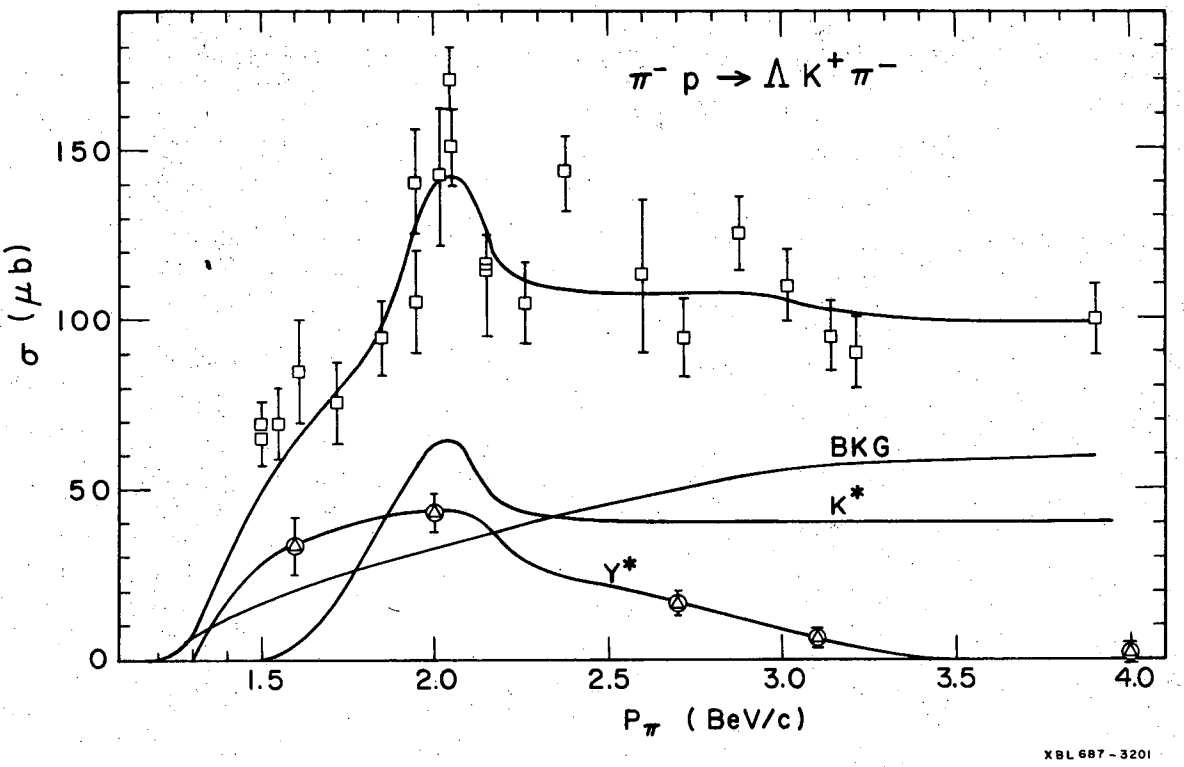
$\pi^- p \rightarrow \Lambda K^+ \pi^-$
150
100
50
0
σ (μb)
1.5
2.0
2.5
3.0
3.5
4.0
P_π (BeV/c)
BKG
K*
Y*
XBL 687-3201

Fig. 8

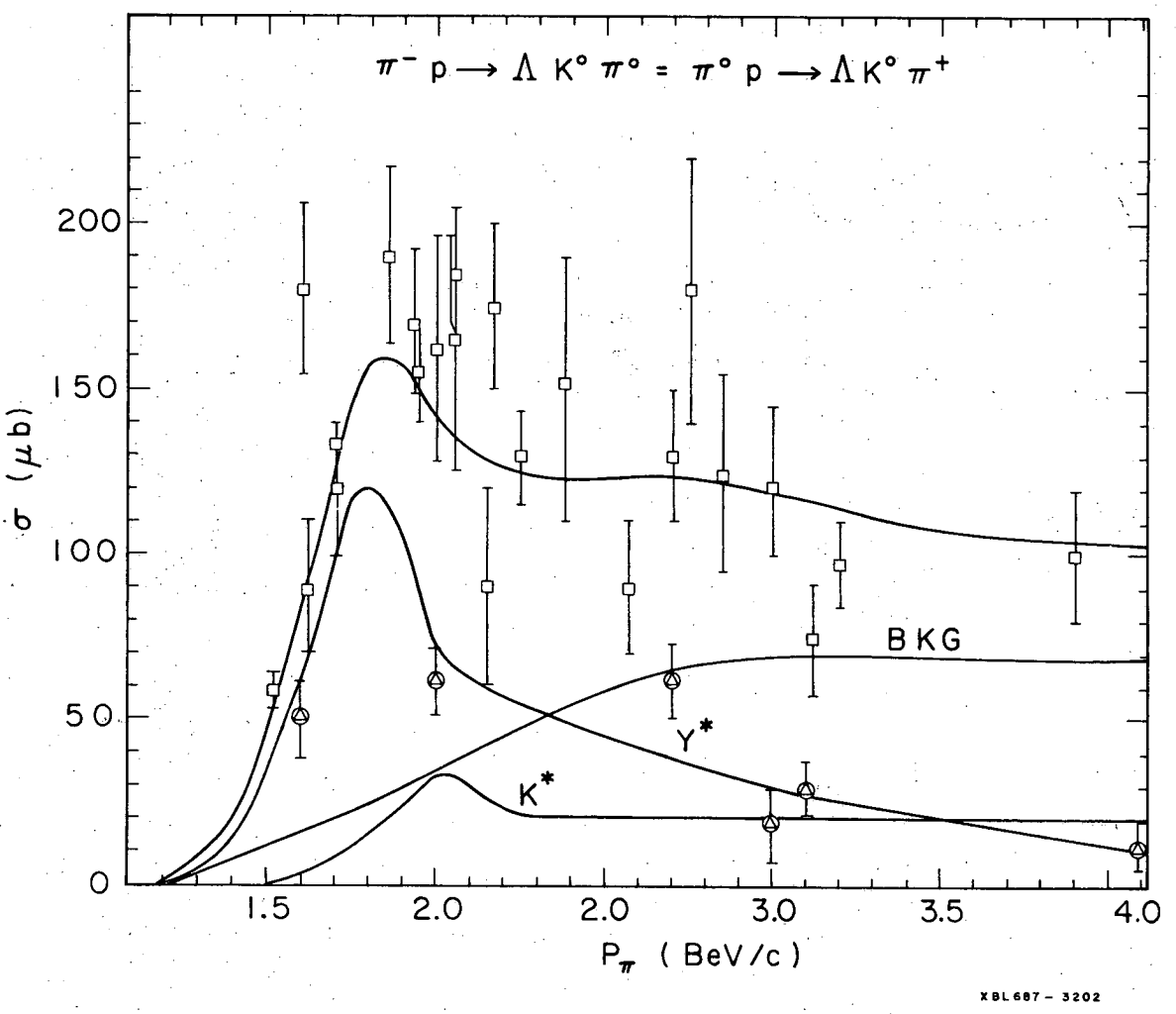
$\pi^- p \longrightarrow \Lambda K^\circ \pi^\circ = \pi^\circ p \longrightarrow \Lambda K^\circ \pi^+$
200
150
100
50
0
σ (μb)
BKG
Y*
K*
1.5
2.0
2.0
3.0
3.5
4.0
P_π (BeV/c)
XBL687 - 3202

Fig. 9

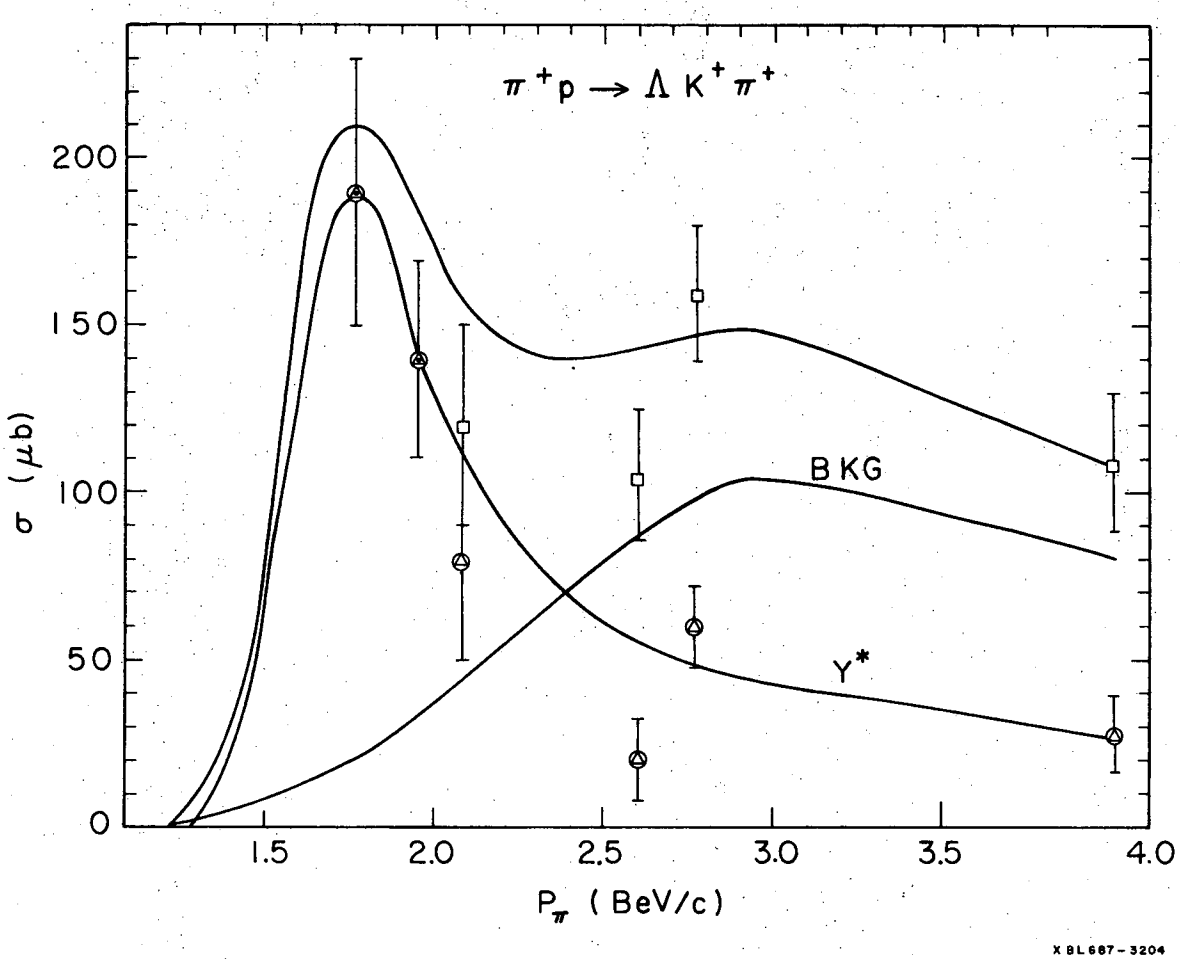
$\pi^+ p \rightarrow \Lambda K^+ \pi^+$
200
150
100
50
0
σ (μb)
BKG
Y*
1.5
2.0
2.5
3.0
3.5
4.0
P_π (BeV/c)
X BL 687-3204

Fig. 10

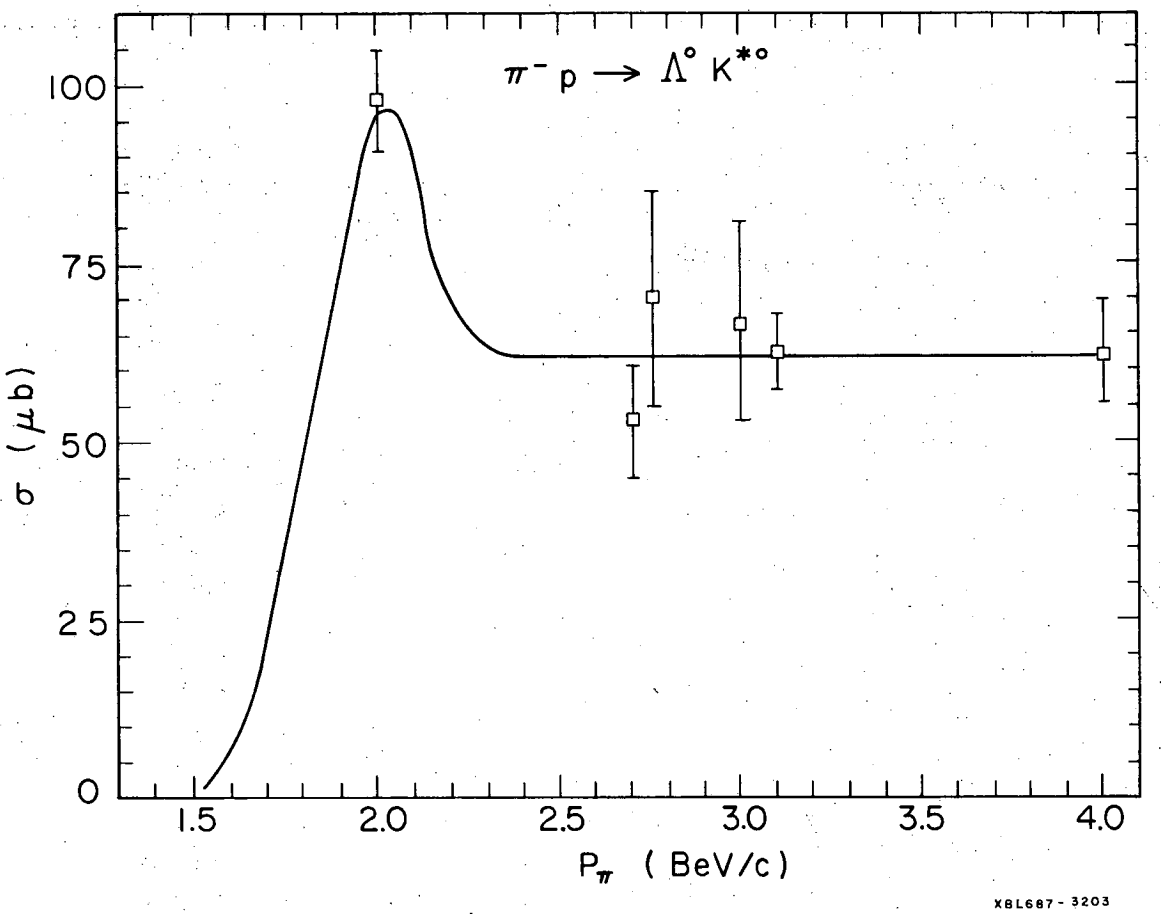
$\pi^- p \rightarrow \Lambda^\circ K^{*\circ}$
100
75
50
25
0
σ (μb)
1.5
2.0
2.5
3.0
3.5
4.0
P_π (BeV/c)
XBL687-3203

Fig. 11

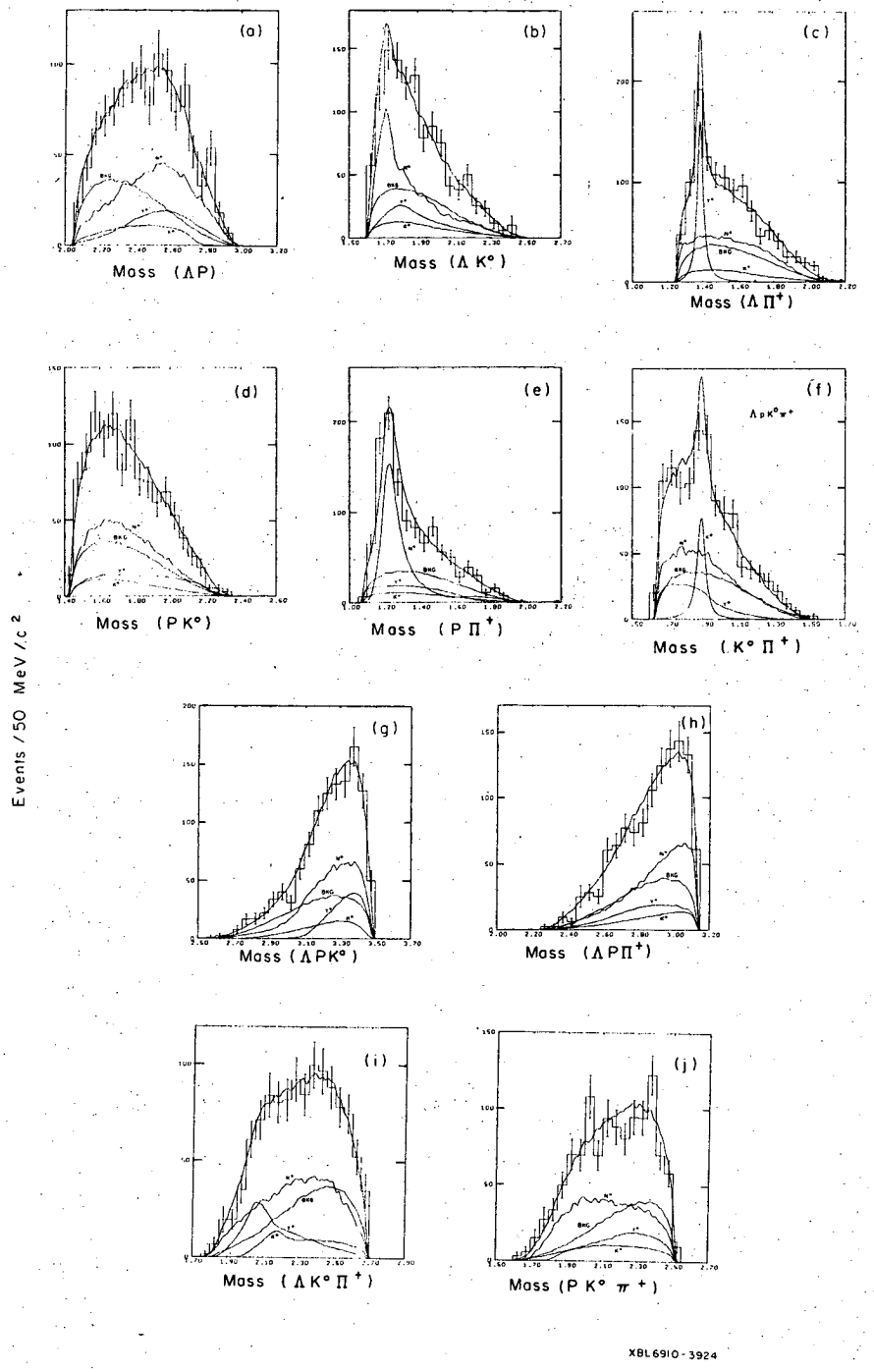
(a)
Mass (ΛP)
(b)
Mass (Λ K°)
(c)
Mass (Λ Π⁺)
(d)
Mass (P K°)
(e)
Mass (P Π⁺)
(f)
ΛpK°π⁺
Mass (K° Π⁺)
Events / 50 MeV/c²
(g)
Mass (ΛPK°)
(h)
Mass (ΛPΠ⁺)
(i)
Mass (Λ K° Π⁺)
(j)
Mass (P K° π⁺)
XBL6910-3924

Fig. 12

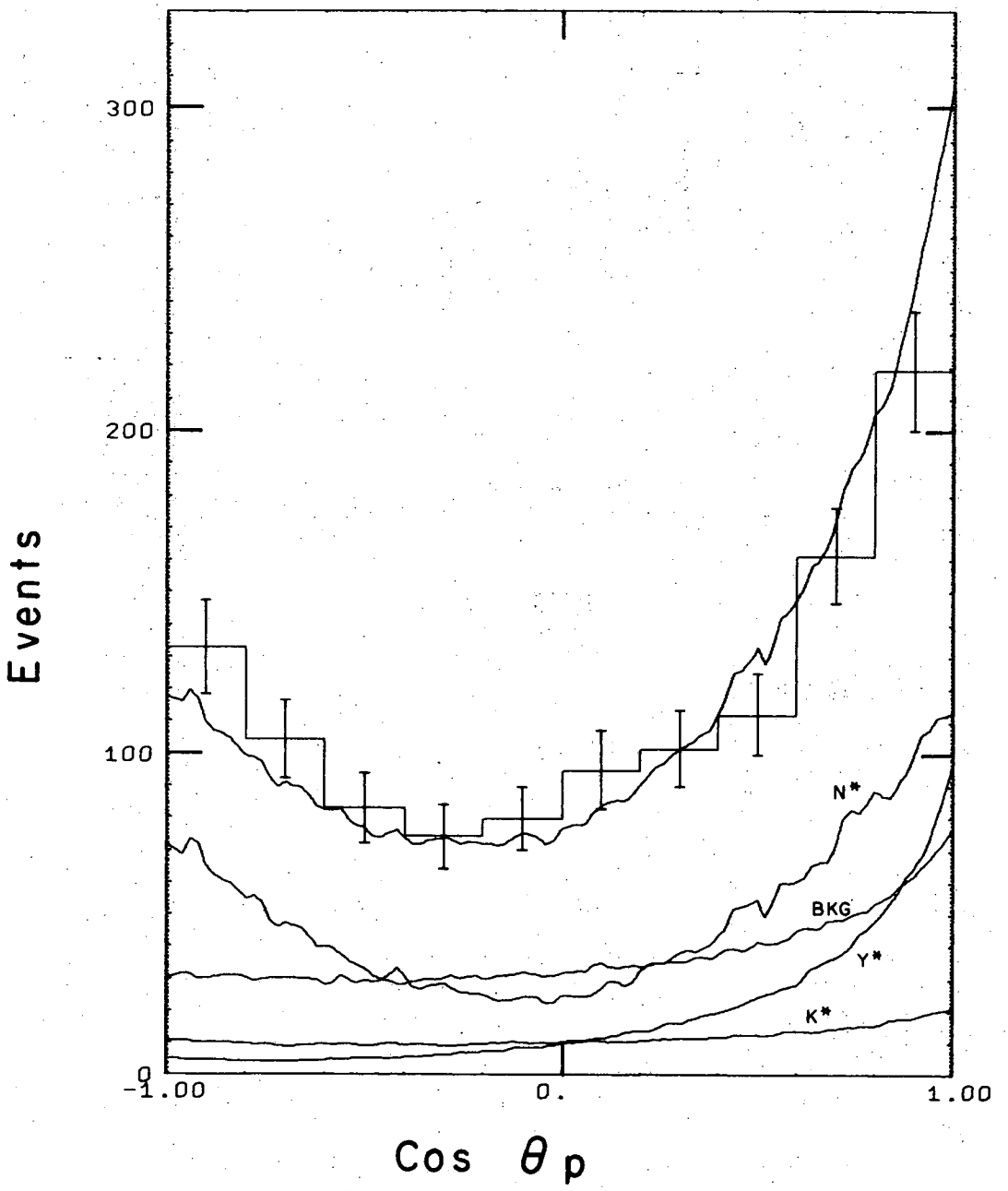

Fig. 13

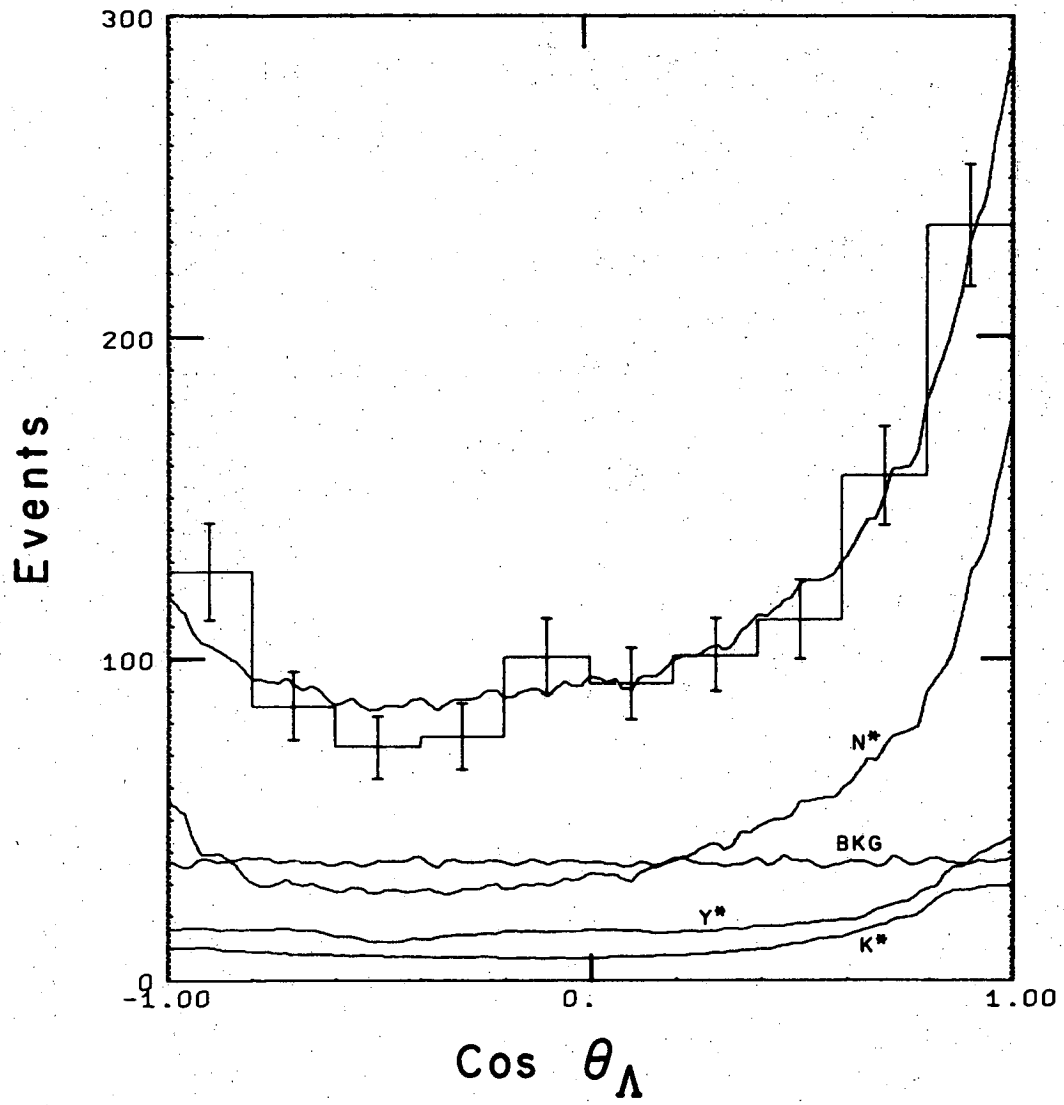

XBL684-543

Fig. 14

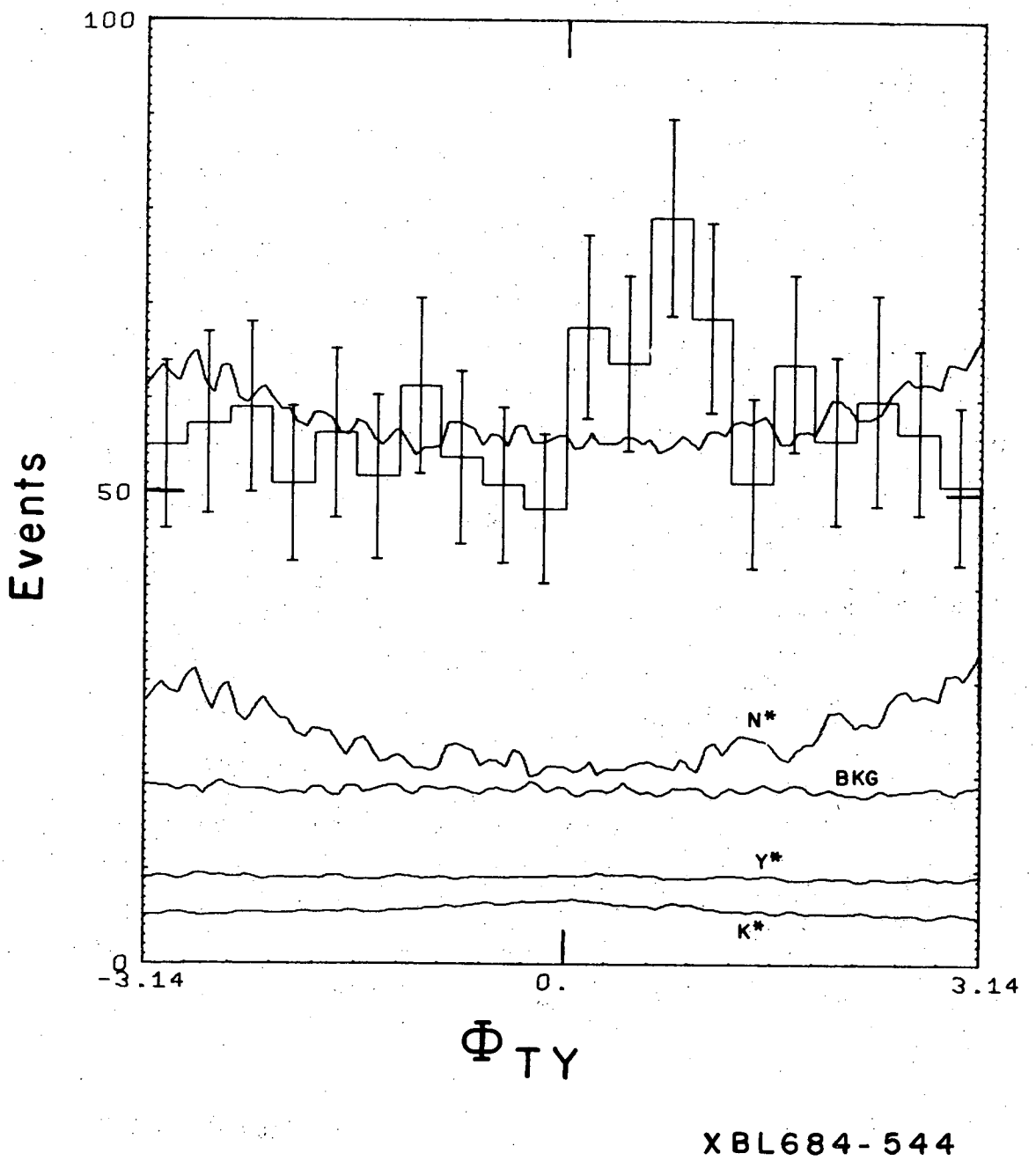

Fig. 15

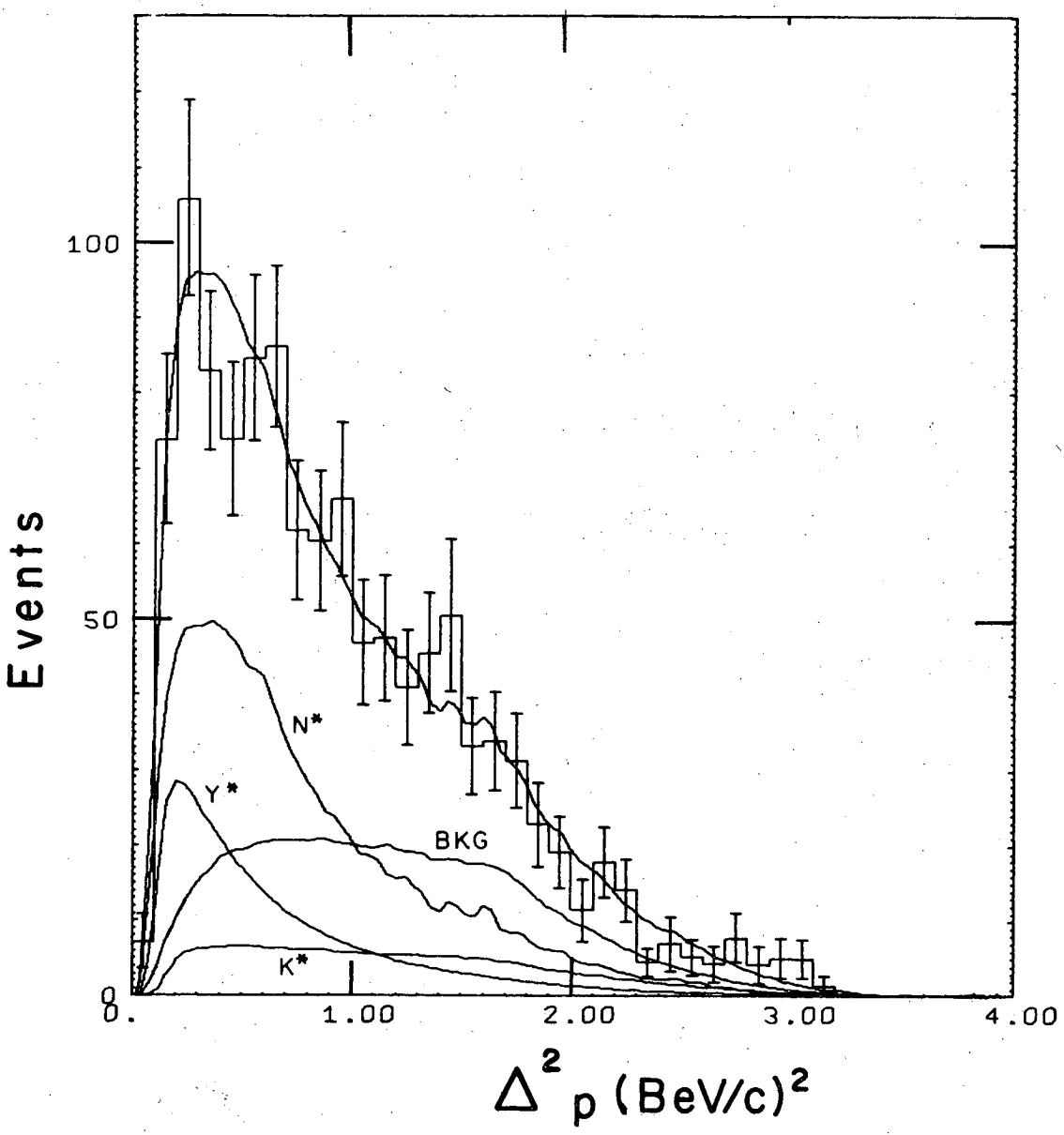

Fig. 16

TECHNICAL INFORMATION DIVISION
LAWRENCE RADIATION LABORATORY
UNIVERSITY OF CALIFORNIA
BERKELEY, CALIFORNIA 94720